

PROPERTIES OF POLYURETHANE FIBROUS MATERIALS PRODUCED BY SOLUTION BLOW SPINNING

Iwona Łopianiak*, Michał Wojasiński, Beata Butruk-Raszeja

Warsaw University of Technology, Faculty of Chemical and Process Engineering,
Waryńskiego 1, 00-645 Warsaw, Poland

The study aimed to produce nano- and microfibrinous materials from polyurethane (ChronoFlex® C75A/C75D in 1,1,1,3,3,3-hexafluoro-2-propanol) by solution blow spinning. Experiments were carried out in order to determine the impact of solution blow spinning parameters on fibre diameter and quality of produced materials. The following properties of produced fibre scaffolds were investigated: fibre size, porosity and pore size, wettability, and mechanical properties. The results confirmed that produced nano- and microfibrinous materials could be potentially used as scaffolds in three-dimensional cell and tissue cultures.

Keywords: nano- and microfibres, 3D cell culture, solution blow spinning, polyurethanes, scaffolds

1. INTRODUCTION

A monolayer covered with medium is the most popular method of cell culture. It has many advantages, such as optimal growth conditions, good availability of biological material, and high repeatability of results. Unfortunately, this method of cell culture can lead to changes in cell morphology, physiology, proliferation, and expression of cell genes and proteins (Bhattacharya et al., 2013; Kitel et al., 2013).

Three-dimensional (3D) cell culture involves growing cells on synthetic supports called scaffolds. The main role of scaffolds for 3D cell culture is to provide cells with an environment close to *in vivo* conditions (Edmondson et al, 2014). Scaffolds are usually made of highly porous biomaterials and act as templates for cell culture or tissue regeneration. They replace the extracellular matrix (ECM), which creates a three-dimensional network of macromolecules supporting cells and mediating the transmission of signals between them (Theocharis et al., 2016). The highly porous structure of scaffolds ensures cells to penetrate the scaffold and provides nutrient transport (Edmondson et al, 2014; Kim, 2005). Thereby, cell-cell, cell-ECM interactions, and cell morphology are close to cell behaviour *in vivo*. Tissue engineering techniques use scaffolds to regenerate various types of tissues, among others: bone, cartilage, ligaments, skin, blood vessels, nerves, and muscles (Chanjuan and Yonggang, 2016). Many of human tissues obey hierarchical structure (from micro- to nanoscale). Therefore, it is important to provide nano- and microstructures (or not unitary structures) for 3D cell culture and tissue engineering (Jun et al., 2018).

It is not possible to produce a universal scaffold enabling the growth of any tissue. The most commonly used materials for producing scaffolds are polymers. They are distinguished by various properties that can be specifically selected depending on the type of tissue they are to replace (Yamamoto et al., 2014). There

* Corresponding author, e-mail: iwona.lopianiak.dokt@pw.edu.pl

are many types of scaffolds and fabrication methods (Behrens et al., 2014; Borden et al., 2014; Hutmacher et al., 2014; Khan et al., 2009; Kurzydłowski and Lewandowska, 2010; Singh et al., 2016; Subbiah et al., 2005).

In this paper, the method for production of nano- and microfibrinous structures as potential scaffolds for three-dimensional cell culture has been presented and described. Also, the impact of selected process parameters on the properties of the final product has been analysed.

2. MATERIALS AND METHODS

2.1. Materials fabrication

Nano- and microfibrinous structures were produced from polyurethanes ChronoFlex C75A (C75A) and ChronoFlex C75D (C75D) (AdvanSource Biomaterials). Nanofibrinous (nanofibres) means that average fibre diameter of produced material was less than 1 μm , while microfibrinous (microfibres) means that average fibre diameters in the material was greater than 1 μm . Two types of materials produced from polymers differing in hardness (75A and 75D in Shore scale) were examined. Polymers were dissolved in 1,1,1,3,3,3-hexafluoroisopropanol (> 99.0%, TCI Chemicals). Polymer solutions were prepared in concentrations 2, 3, 4, 6, 6.5, 7, 7.5, 8 and 8.5% w/w for C75A polymer and 2, 3, 4, 7, 7.5, 8, 8.5 and 9% w/w for C75D polymer; the solutions were stirred overnight prior to the spinning process.

Fibrous materials were fabricated using solution blow spinning (SBS) process. SBS setup is shown in Fig. 1. The main part of this setup is the concentric nozzle system. The polymer solution was supplied through the inner nozzle, while the compressed gas (air) was supplied through the outer nozzle. The polymer solution flow rate was controlled with the syringe pump (KDS 100, KDS Scientific Inc., USA). The driving force of the SBS process is a high-speed compressed dry airflow. The polymer solution was formed by the compressed air and dragged towards the collector. The working distance was fixed at 30 cm, and the speed of the collector was 3000 rpm.

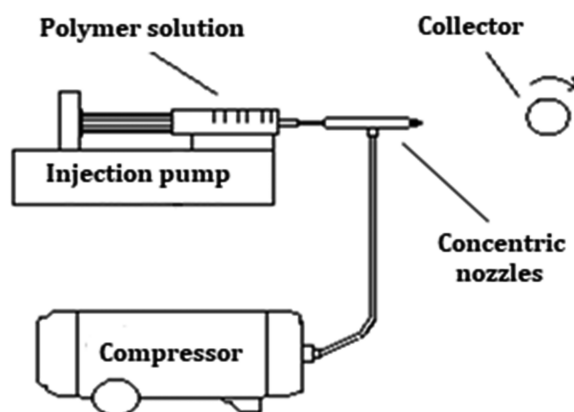


Fig. 1. Solution blow spinning setup

Materials were fabricated at polymer solution flow rates: 10, 15, 20, 25, 30, 40, 50 ml/h and at gas pressures: 0.1, 0.125, 0.15, 0.175, 0.2 MPa. Various combinations of polymer concentration, gas pressure, and polymer solution flow rate permitted to find the best parameters to produce materials with a minimum number of defects. We obtained mainly nanofibers with 2% polymer solution used, and mainly microfibers for blow spinning of 8% polymer solution.

2.2. Scaffold characterization

2.2.1. Fibre diameter, pore size, porosity

Samples ($n = 3$) of each produced material were coated with a 15 nm layer of gold using a sputter coater (K550 Emitech, Quorum Technologies) and subjected to scanning electron microscopy (SEM, Phenom G1, PhenomWorld). Samples were photographed in 200 \times , 600 \times , 5000 \times or 7500 \times magnification. Images were used for fibre diameter ($n = 100$ fibre diameters were measured for each material), and pore size ($n = 50$ pore sizes were measured for each material) measurements using Fiji software (Schindelin et al., 2012) and for sample surface evaluation. Average fibre diameter and average pore size were determined as an arithmetic mean value of all measurements. The porosity of the materials, η , was determined using the formula:

$$\eta = 1 - \frac{\rho_s}{\rho_p} \quad (1)$$

where:

$$\rho_s = \frac{m}{S \cdot \delta} \quad (2)$$

$\rho_p = 1200 \text{ kg/m}^3$ (Padsalgikar, 2017).

To determine density and then porosity of the produced materials, three square-shaped samples of each material ($n = 3$) with dimensions of about 1 cm \times 1 cm were used. Their dimensions were accurately measured, and the average area (S) was calculated. Each sample was weighed (m) on an analytical balance, and then a narrow strip ($n = 1$) was cut, glued vertically to the SEM microscope stub and images ($n = 5$ for each sample) at 300 \times magnification were taken. Images were used to determine the thickness (δ) of materials using Fiji software, $n = 25$ measurements of material thickness were made. Results are presented as a mean value \pm SD.

2.2.2. Number of surface defects

SEM material images ($n = 5$) in magnification of 200 \times were used to count the number of surface defects. Nodules, spindles, and stains were defined as defects. Various surface defects are shown in Fig. 2. Defects were counted from the central part of the image, and the top and right edge.

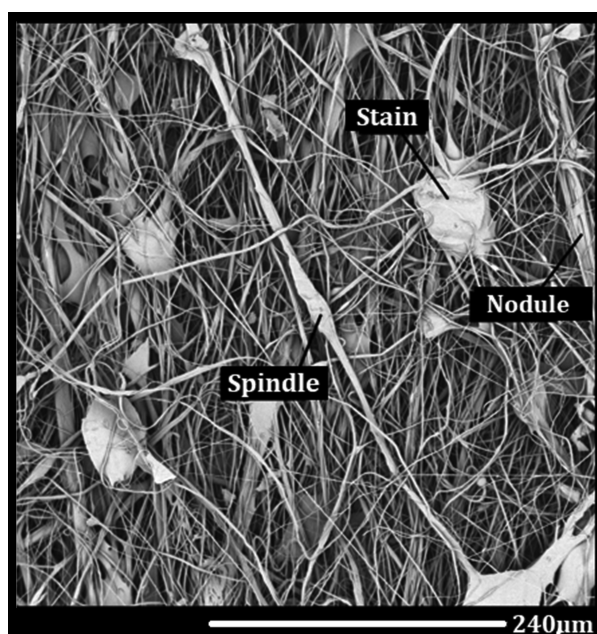


Fig. 2. Defect classification scheme

2.2.3. Wettability

Material wettability was measured using a drop shape analyser (DSA–100s, KRÜSS) controlled by Krüss ADVANCE computer software. The contact angle between liquid and solid was measured. Samples ($n = 3$) of each material were glued to a glass slide, and then a drop (5 μl) of distilled water was placed on it. The contact angle of $n = 10$ drops was measured for each sample. Results are presented as a mean value \pm SD.

2.2.4. Mechanical properties

Materials were analysed in the form of a 5 mm width and a 5 cm long flat samples. They were placed in the holders of the Instron 3345 testing machine and stretched at a rate of 5 mm/min following ASTM D638-02a. Computer software enabling control of the testing machine automatically determined the Young's Modulus, elongation at break, and ultimate tensile stress for a porous sample. $n = 5$ samples of each material were analysed. Results are presented as a mean value \pm SD.

Ultimate tensile stress for porous sample, σ_{por} , was determined using the formula:

$$\sigma_{por} = \frac{F_{\max}}{A(1 - \eta)} \quad (3)$$

Young's modulus, E , was determined using the formula:

$$E = \frac{\sigma_{por}}{\varepsilon}, \quad \varepsilon = \frac{\Delta L}{L_0} \quad (4)$$

3. RESULTS

3.1. Best process parameters

3.1.1. Fibre diameter

Fibre diameter measurement results for various concentrations of polymer solutions are shown in Fig. 3.

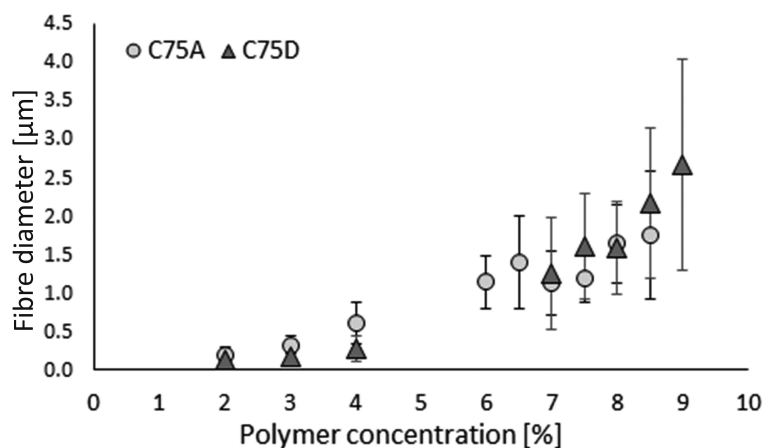


Fig. 3. Average fibre diameter ($n = 100$) in the function of polymer solution concentration

The study aimed to produce two types of fibrous materials: microfibrinous with average fibre diameter $d \geq 1 \mu\text{m}$ and nanofibrinous with average fibre diameter $d \leq 1 \mu\text{m}$ ($d \approx 0.25 \mu\text{m}$). Based on the diameter measurement, polymer concentrations of 2% (C75A) and 3% (C75D) were selected for further fabrication and analysis of nanofibres. Simultaneously polymer concentration of 8% (C75A and C75D) were selected for further fabrication and analysis of microfibrinous.

3.1.2. Number of surface defects

The conducted tests revealed that two parameters, namely compressed air pressure and polymer solution flow rate, exerted a significant impact on the number and the size of surface defects. In the case of samples with a very large number of defects, difficult to count, the sign ∞ was used.

In the case of microfibrinous materials, it was not possible to produce materials at a compressed air pressure below 0.1 MPa due to the very high viscosity of polymer solutions. The results of the analysis of surface defects are shown in Table 1.

Table 1. Number of surface defects obtained at different compressed air pressure and different polymer solution flow rates

		Number of defects			
		C75A 2%	C75D 3%	C75A 8%	C75D 8%
Compressed air pressure [MPa]	0.05	46	26	–	–
	0.075	38	14	–	–
	0.1	34	34	39	37
	0.125	48	23	35	52
	0.15	51	29	38	50
	0.175	46	42	39	∞
	0.2	∞	34	50	∞
Polymer solution flow rate [ml/h]	10	45	41	39	43
	15	32	33	32	36
	20	34	32	45	45
	25	36	46	48	40
	30	37	36	35	37
	40	47	42	32	∞
	50	46	32	31	∞

In addition to the number, the defect sizes were also taken into account. A detailed analysis of all surface images, together with the number of defects, allowed to find the optimal values of compressed air pressure and polymer solution flow rate. The results of the analysis are shown in Table 2.

Table 2. The parameters selected to produce fibrous materials with the desired properties

Process parameters	Type of polymer			
	C75A		C75D	
	nanofibres	microfibres	nanofibres	microfibres
Polymer solution concentration [%]	2	8	3	8
Compressed air pressure [MPa]	0.1	0.1	0.1	0.1
Polymer solution flow rate [ml/h]	30	30	30	30

3.2. Pore size and porosity

Results of porosity and pore size measurements are shown in Figs. 4. and 5.

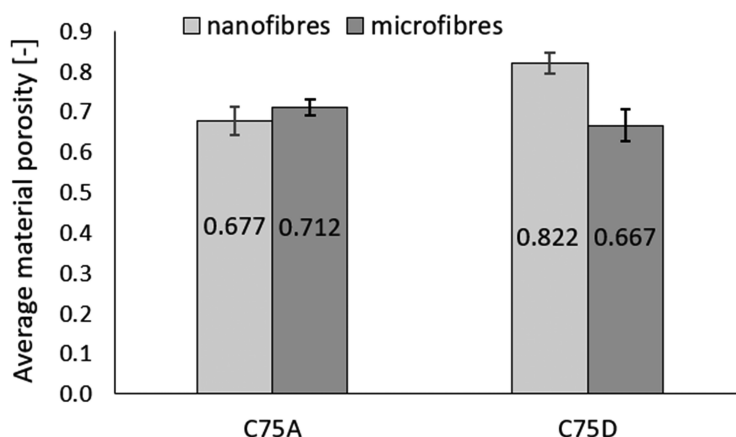


Fig. 4. Porosity measurement results ($n = 3$)

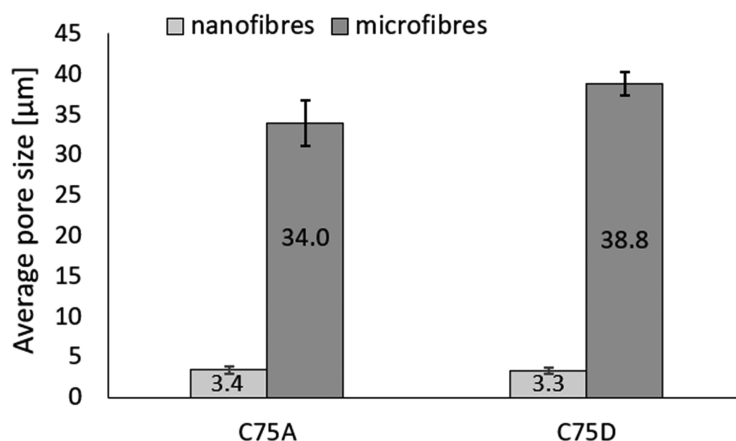


Fig. 5. Pore size measurement results ($n = 50$)

The porosity of nanofibres produced from C75D is higher than that of microfibres. This is because when the average fibre size is reduced, the specific surface area of the material increases and thus its porosity. In the case of C75A, the porosity of nanofibres is similar to the porosity of microfibres. No change in material porosity can explain its high elasticity. Stretched elastic nanofibres shrink after removal from the collector, which reduces the pore volume, and slightly increases the diameter of fibres, leading to a decrease of the material porosity.

Regardless of the type of polymer, the values of pore sizes for nanofibrous and microfibrinous materials were similar. The average pore size in microfibrinous materials is about ten times larger than in nanofibrous materials. The relationship observed for the average fibre diameter is visible in a similar way for the pore sizes (both characteristics take values about 10 times higher for microfibrinous materials). Thus, increasing the fibre size results in the expected increase in pore size in the produced materials (Eichhorn and Sampson, 2005).

3.3. Wettability

The results of wettability analysis are shown in Fig. 6.

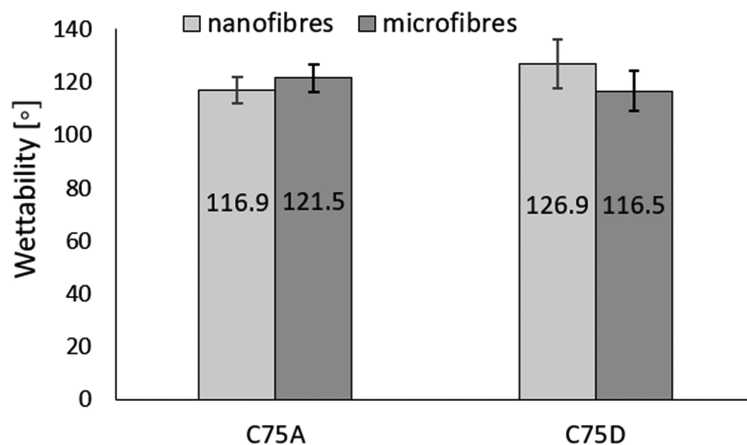


Fig. 6. Wettability test results (n = 10)

The values of contact angles do not differ significantly for all four material variants. Based on the obtained contact angle values it can be stated that the produced fibrous materials are hydrophobic. In order to use materials as scaffolds in a three-dimensional cell culture, their surface should be modified (Safinia et al., 2005).

3.4. Mechanical properties

The analysis of the mechanical properties is shown in Table 3.

Table 3. Mechanical properties of fabricated materials

Polymer	Polymer solution concentration	Young’s modulus ±SD [MPa]	Elongation at break ±SD [%]	Ultimate tensile stress for porous sample ±SD [MPa]
C75A	2%	2.9 ± 0.4	63.4 ± 7.3	4.3 ± 0.4
	8%	0.6 ± 0.1	156 ± 17.5	2.3 ± 0.2
C75D	3%	4.7 ± 0.4	27.3 ± 2.9	2.4 ± 0.2
	8%	64.1 ± 10.1	20.2 ± 2.0	5.8 ± 0.6

In general, materials produced from C75A polymer have a lower Young’s modulus values than materials made of C75D polymer. Therefore, materials produced from C75A polymer are more flexible than materials produced from C75D polymer. This was also reflected by the values of the elongation at break. Samples made from C75A achieve much higher elongation at break values than samples fabricated from C75D.

The highest value of ultimate tensile stress for porous samples for C75D 8% material exhibits the best mechanical properties. C75D 3% materials are the least resistant to stretch. In the case of elastic materials (produced from C75A), better mechanical properties were exhibited by nanofibrous materials. In general, all produced materials present mechanical properties appropriate for use in biomedical applications.

4. CONCLUSIONS

The selection of appropriate process parameters allowed the production of fibres of the desired size and required quality (the smallest number and size of defects). The research showed that the concentration of the polymer solution had a significant impact on the size of fibres. The average fibre diameter increased when the polymer solution concentration increased.

The analysis of the surface of produced samples proved that compressed air pressure and polymer solution flow rate strongly influenced the quality (number and size of defects) of fibrous materials. During the tests, it was shown that high concentration (high viscosity) of polymer solutions required a higher driving force (compressed air pressure) of the process.

A detailed SEM image analysis of the surfaces allowed to find optimal values of compressed air pressure and polymer solution flow rate. The application of the selected process parameters minimized the size and amount of all types of surface defects and ensured the highest efficiency and the least energy consumption of the process while maintaining its stability. Regardless of the concentration of the polymer solution and the type of polymer, the following process parameters were selected: compressed air pressure of 0.1 MPa and polymer solution flow rate of 30 ml/h.

The nanofibrous material pore size was about ten times smaller than the microfibrillar material pore size for samples made of both types of polymers. It shows that the fibre size of the produced materials strongly influenced the pore size. The porosity of nanofibrous materials produced from C75D polymer was higher than that of microfibrillar materials produced from the same polymer. This is what was expected because as the pore size decreased, the surface area of the material increased and thus its porosity.

The contact angles of all produced fibrous materials are similar for every type of material and amount to about 120°. Thus, the fabricated fibrous materials are hydrophobic.

Analysis of Young's modulus and elongations at break of the samples showed that microfibrillar materials made from C75A polymer were more flexible than materials made from C75D polymer, which confirmed that the mechanical properties of materials strongly depended on the initial hardness of the polymer. Similar ultimate tensile stress for all types of mats suggested that change in the diameter of the fibres in the materials did not affect their mechanical properties.

This work developed a method for producing fibrous materials, which can be used as scaffolds in three-dimensional cell cultures. It has been shown that it is possible to minimize structure defects and change the diameter of the fibres from about 0.2 µm to about 3 µm. Production of two types of nonwovens, with micro- and nanofibres, significantly broadens the spectrum of potential applications of the presented materials.

This work was supported by the National Centre for Research and Development in the LIDER programme and research grant: "BioGraft – biomimetic vascular prostheses of small diameters", Project Contract No. LIDER/18/0104/L-8/16/NCBR/2017.

SYMBOLS

A	sample cross-section area, m ²
E	Young's Modulus, Pa
F_{\max}	maximum force acting on the sample, N
L	sample deformation, m

L_0	initial length of sample, m
ΔL	change of sample length, m
m	sample mass, kg
n	number of measured values, –
S	sample area, m ²

Greek symbols

ε	sample strain, –
η	sample porosity, –
δ	sample thickness, m
ρ_s	sample density, kg/m ³
ρ_p	polymer density, kg/m ³
σ_{por}	ultimate tensile stress for porous sample, Pa

REFERENCES

- ASTM D638 – 02a – *Standard Test Method for Tensile Properties of Plastics*.
- Behrens A.M., Casey B.J., Sikorski M.J., Wu M.J., Tutak K.L., Sandler A.D., Kofinas P., 2014. In situ deposition of PLGA nanofibres via solution blow spinning. *ASC Macro Letters*, 3, 249–254. DOI: [10.1021/mz500049x](https://doi.org/10.1021/mz500049x).
- Bhattacharya M., Malinen M.M., Lauren P., Lou Y., Kuisma S.W., Kanninen L., Lille M., Corlu A., GuGuen-Guillouzo C., Ikkala O., Laukkanen A., Urtti A., Yliperttula M., 2013. Nanofibrillar cellulose hydrogel promotes three-dimensional liver cell culture. *J. Controlled Release*, 164, 291–298. DOI: [10.1016/j.jconrel.2012.06.039](https://doi.org/10.1016/j.jconrel.2012.06.039).
- Borden M., Attawia M., Khan Y., Laurencin C.T., 2002. Tissue engineered microsphere – based matrices for bone repair, design and evaluation. *Biomaterials*, 23, 551–559. DOI: [10.1016/S0142-9612\(01\)00137-5](https://doi.org/10.1016/S0142-9612(01)00137-5).
- Chanjuan D., Yonggang L.V., 2016. Application of collagen scaffold in tissue engineering: Recent advances and new perspectives. *Polymers*, 8, 42–56. DOI: [10.3390/polym8020042](https://doi.org/10.3390/polym8020042).
- Edmondson R., Broglie J.J., Adcock A.F., Yang L., 2014. Three-dimensional cell culture systems and their applications in drug discovery and cell-based biosensors. *ASSAY Drug Dev. Technol.* 12(3), 207–218. DOI: [10.1089/adt.2014.573](https://doi.org/10.1089/adt.2014.573).
- Eichhorn S.J., Sampson W.W., 2005. Statistical geometry of pores and statistics of porous nanofibrous assemblies. *J. R. Soc. Interface*, 2, 309–318. DOI: [10.1098/rsif.2005.0039](https://doi.org/10.1098/rsif.2005.0039).
- Hutmacher D.W., Woodfield T.B.F., Dalton P.D., 2015. Scaffold Design and Fabrication. In: van Blitterswijk C., De Boer J. (Eds.), *Tissue Engineering*. 2nd edition, Academic Press, 311–346.
- Indong J., Han H. S., Edwards J. R., Jeon H., 2018. Electrospun Fibrous Scaffolds for Tissue Engineering: Viewpoints on Architecture and Fabrication. *Int. J. Mol. Sci.*, 19, 745. DOI: [10.3390/ijms19030745](https://doi.org/10.3390/ijms19030745).
- Kim J.B., 2005. Three-dimensional tissue culture models in cancer biology. *Semin. Cancer Biol.*, 365–377. DOI: [10.1016/j.semcancer.2005.05.002](https://doi.org/10.1016/j.semcancer.2005.05.002).
- Kitel J., Czarnecka J., Rusin A., 2013. Trójwymiarowe hodowle komórek – zastosowania w badaniach podstawowych i inżynierii tkankowej. *Postępy Biochemii*, 59, 305–321.
- Khan F., Tare R.S., Oreffo R.O. C., Bradley M., 2009. Versatile biocompatible polymer hydrogels: Scaffolds for cell growth. *Angew. Chem. Int. Ed.*, 48, 978–982. DOI: [10.1002/anie.200804096](https://doi.org/10.1002/anie.200804096).
- Kurzydłowski K., Lewandowska M., 2010. *Nanomateriały inżynierskie konstrukcyjne i funkcjonalne*. Wydawnictwo Naukowe PWN, 256–284.
- Padsalgikar A.D., 2017. *Plastics in medical devices for cardiovascular applications*. William Andrew, Elsevier Inc., United Kingdom, 64. DOI: [10.1016/B978-0-323-35885-9.00003-5](https://doi.org/10.1016/B978-0-323-35885-9.00003-5).
- Safinia L., Datan N., Hohse M., Mantalaris A., Bismarck A., 2005. Towards a methodology for the effective surface modification of porous polymer scaffolds. *Biomaterials*, 26, 7537–547.

- Singh M.R., Patel S., Singh D., 2016. Natural polymer-based hydrogels as scaffolds for tissue engineering. In: Grumezescu A.M. (Ed.), *Nanobiomaterials in soft tissue engineering. Applications of Nanobiomaterials Volume 5*. William Andrew Applied Science Publishers. 231–260. DOI: [10.1016/B978-0-323-42865-1.00009-X](https://doi.org/10.1016/B978-0-323-42865-1.00009-X).
- Subbiah T., Bhat G.S., Tock R.W., Parameswaran S., Ramkumar S.S., 2005. Electrospinning of nanofibers. *J. Appl. Polym. Sci.*, 96, 557–569. DOI: [10.1002/app.21481](https://doi.org/10.1002/app.21481).
- Schindelin J., Arganda-Carreeras Frise E., Kaynig V., Lingair M., Pierzsch T., Preibisch S., Rueden C., Saalfeld S., Schmdt B., Tinevez J., White D.J., Hartenstein V., Eliceiri K., Tomancak P., Cardona A., 2012. Fiji: an open-source platform for biological-image analysis. *Nature Methods*, 28, 676–682. DOI: [10.1038/nmeth.2019](https://doi.org/10.1038/nmeth.2019).
- Theocharis A.D., Skandalis S.S., Gialeli C., Karamanos N.K., 2016. Extracellular matrix structure. *Adv. Drug Delivery Rev.*, 97, 4–27. DOI: [10.1016/j.addr.2015.11.001](https://doi.org/10.1016/j.addr.2015.11.001).
- Yamamoto M., Rafii S., Rabbany S. Y., 2014. Scaffold biomaterials for nano-pathophysiology. *Adv. Drug Delivery Rev.*, 74, 104–114. DOI: [10.1016/j.addr.2013.09.009](https://doi.org/10.1016/j.addr.2013.09.009).

Received 29 April 2020

Received in revised form 9 November 2020

Accepted 18 November 2020